Journal of the European Ceramic Society xxx (xxxx) xxx–xxx

Contents lists available at ScienceDirect

Journal of the European Ceramic Society

journal homepage: www.elsevier.com/locate/jeurceramsoc

Original Article

On the Yttrium Tantalate – Zirconia phase diagram

Mary Gurak[1], Quentin Flamant, Laetitia Laversenne[2], David R. Clarke*

John Paulson Harvard School of Engineering and Applied Sciences, Harvard University, Cambridge, MA 02138, USA

ARTICLE INFO

Keywords:
Phase equilibria
Zirconia
Yttrium tantalate
Phase transformations
Thermal barrier coatings

ABSTRACT

The phase diagram for the $YTaO_4$-ZrO_2 quasi-binary has been determined up to 1600 °C. There are three distinct compositional regimes: an extensive $YTaO_4$ solid solution, an extensive ZrO_2 solid solution and a two-phase intermediate region. The addition of ZrO_2 to $YTaO_4$ decreases the *M–T* transition temperature almost linearly from 1426 °C to approximately 450 °C at the solubility limit (~28 mol% ZrO_2), and then remains constant until the ZrO_2 solid solution phase boundary is reached. Within the intermediate region, there exists an extensive two-phase tetragonal (*T* + *t*) phase field above the M–T transformation temperature. The transformation exhibits no hysteresis on heating and cooling but nonetheless there is a distribution with temperature in the mass fraction of the monoclinic and tetragonal phases so no unique transformation temperature can be identified. No other high temperature phases were observed but it is suggested that a higher temperature solid solution phase is likely above 1700 °C, based on the similarity in crystallographic relationship between the two tetragonal solid solution structures.

1. Introduction

It is widely recognized in the turbine materials community that the engine efficiency, whether for power generation or propulsion, increases with the high-temperature turbine inlet temperature [1]. Over the years since the first gas turbines were built there have been several developments that have enabled designers to meet the challenge of increasing temperatures. These include the development of single crystals of metal alloy compositions capable of higher temperature creep and fatigue resistance [2], the use of ever more complicated internal cooling of the turbine blades [3,4] and the introduction of thermal barrier coatings of the blades and vanes [1,5]. Since the introduction of thermal barrier coatings, the material of choice has been, and continues to be, yttria-stabilized zirconia in its' meta-stable tetragonal-prime (*t'*) phase [6,7]. This has a combination of attractive properties: low thermal conductivity [8], high fracture toughness [9] and ease of deposition over complex shapes [7]. Increasingly, as the turbine inlet temperature is being raised further, some of the very highest temperature limitations of this oxide are being recognized. Principal amongst these are the observations that the meta-stable *t'* phase undergoes a slow but temperature-dependent, kinetically-limited transformation to a thermodynamically stable mixture of cubic and tetragonal phases, the latter of which can transform to monoclinic zirconia on cooling [6,10]. The concern with this transformation is that the large accompanying volumetric expansion can cause cracking and accelerated failure of the coating. The kinetics of the meta-stable tetragonal conversion are well described by the Larson-Miller relation even though the actual exponent has been found to depend on the actual measurement made to measure the transformation [6,11]. For engine designers, the importance of the Larson-Miller fitting is that it allows them to estimate the combination of temperatures and times at temperature before the transformation will occur.

Although it is now known that there are many oxides [12] that are capable of withstanding higher temperatures than the meta-stable form of yttria-stabilized zirconia and also have lower thermal conductivity, they lack any intrinsic toughening mechanism. Many can also be difficult to deposit, especially at high rates on curved surfaces. More limited in number are the high-temperature oxides that undergo some form of displacive or martensitic phase transformation at high temperatures. One of these is yttrium tantalate ($YTaO_4$) which early reports suggested had a tetragonal-to-monoclinic transformation at about 1450 °C [13,14], considerably higher than the corresponding transformation temperature in pure zirconia (~1060 °C). Based on several literature reports that the tetragonal form of zirconia can be stabilized by equal concentrations of Y^{3+} and Ta^{5+}, this work reports investigations of the pseudo-binary phase diagram between $YTaO_4$ and ZrO_2, extending previous studies [15] of the phase transformations at the $YTaO_4$ end of the diagram. A further attractive feature of this system is that

* Corresponding author.
E-mail address: clarke@seas.harvard.edu (D.R. Clarke).
[1] Now at: Pratt and Whitney Aircraft, Hartford, CT, USA.
[2] Now at: Institute NEEL CNRS, 38042 Grenoble, France.

https://doi.org/10.1016/j.jeurceramsoc.2018.03.012
Received 21 January 2018; Received in revised form 9 March 2018; Accepted 9 March 2018

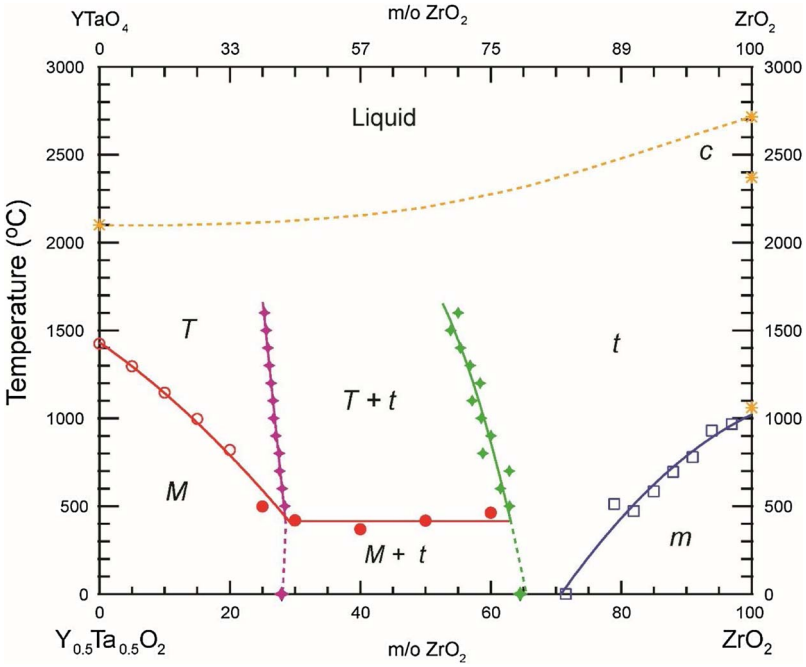

Fig. 1. Phase diagram along the $YTaO_4$–ZrO_2 quasi-binary. The filled markers correspond to this work, and the open markers are data from literature including our own [1,5,8]. The room temperature solubility limits are marked by the vertical dashed lines. For convenience, the compositions are indicated both in terms of molar mixtures of $YTaO_4$ and ZrO_2 (top) and in terms of constant number of cations and anions (bottom), the notation used in this work.

fully-dense compositions along this join have considerably lower thermal conductivities than that of 8YSZ [16].

The majority of previously reported phase diagram studies have focused on the zirconia-rich end of the $YTaO_4$-ZrO_2 diagram, Fig. 1. Complementary studies by XRD [17–19], Raman [20] and dilatometry in this compositional region indicate that co-doping with equal amounts of Y^{3+} and Ta^{5+} decreases the tetragonal-monoclinic (*t-m*) transformation temperature monotonically with concentration up to about 25 m/o $YTaO_4$ substitution into ZrO_2. Over this compositional range the tetragonal phase can be retained on cooling depending on the grain sizes and cooling rates otherwise it transforms martensitically to a monoclinic zirconia solid solution [20]. At the other end of the pseudo-binary, $YTaO_4$, previous studies [15] of the phase stability show that ZrO_2 can substitute into $YTaO_4$ up to at least a concentration of 25 m/o ZrO_2. Over this compositional range the *T-M* phase transformation temperature decreases from 1426 °C for pure $YTaO_4$ down to ~500 °C [15]. Most significantly for potential toughening, the transformation is purely displacive over the entire solid solution [15,21]. Intriguingly, the XRD studies of the tetragonal-monoclinic (*T-M*) transformation in the single-phase $YTaO_4$ solid solution region also indicate that a proportion of the tetragonal (*T*) phase can be retained on cooling of the powders to room temperature [15]. This is analogous to the retention of the *t'* tetragonal prime phase on cooling at the ZrO_2 end of the diagram.

Preliminary microstructural observations and room temperature XRD measurements suggest that even though both the $YTaO_4$ solid solution and the ZrO_2 solid solutions are tetragonal, there exists a two-phase co-existence region between them. The work presented in this contribution describes the determination of the compositional limits of the two solid solutions and the phase transformation behavior in the two-phase region. As the kinetics in this system are very slow, the emphasis in this work has been on X-ray measurements primarily carried out on powders, rather than bulk samples, in air at high temperatures. The slow grain growth kinetics in this material system is evident from the grain size in dense samples even after being held at 1600 °C for 40 h, as shown in Fig. 2.

To avoid confusion, the tetragonal and monoclinic forms of the zirconia-solid solution phases are indicated by the lower case letters *t-* and *m-*, respectively, whereas those of the yttrium-tantalate solid solution are indicated by the upper case letters *T-* and *M-*. Compositions are expressed in this work in terms of mole percent of single cation formula units, namely as $Y_{(1-x)/2}Ta_{(1-x)/2}Zr_xO_2$ so the terminal phases are $Y_{0.5}Ta_{0.5}O_2$ (x = 0) and ZrO_2 (x = 1).

2. Experimental details

The majority of our studies have been performed on fine powders prepared by the reverse co-precipitation method [15,22,23]. Mixed cation solutions were prepared from zirconium oxy-nitrate hydrate (> 99%) and yttrium nitrate hexahydrate (> 99.8%) aqueous solutions mixed with tantalum chloride (99.99%) solutions in ethanol, with the concentrations calibrated using the gravimetric method. The mixed solution was then added drop-by-drop into an ammonium hydroxide solution at an initial pH of 11.2 at room temperature, stirring the whole time and with the pH maintained above 10.6. White precipitates were formed and then separated by centrifugation. These were subsequently washed three times, twice with deionized (DI) water and once with ethanol, before being dried overnight. Finally, the powders were calcined in air at 700 °C for 2 h to create molecularly mixed metal oxides. Based on DSC studies, the powders crystallize to the monoclinic-prime phase at temperatures dependent on the ZrO_2 content. These then transformed to the equilibrium phases at higher temperatures, as confirmed by Raman spectroscopy. For the X-ray diffraction (XRD) studies presented in this work, all the calcined powders were first heated at 1600 °C for 40 h so that they became tetragonal. These conditions were selected based on preliminary measurements.

Phase identification was performed by X-ray diffraction using different facilities. The highest angular resolution measurements at room temperature were made at the Advanced Photon Source (APS) at Argonne National Laboratory (in Argonne, Illinois, USA) using the 11-BM mail-in program. Prior to making these measurements, the calcined powders underwent different heat treatments before being ground with a mortar and pestle and then passed through a 325 mesh sieve. The X-ray wavelength was 0.459981 Å (27 keV).

High temperature diffraction studies of the 25 mol% ZrO_2 and 30 mol% ZrO_2 compositions were performed up to 1000 °C using a PANalytical X'Pert PRO diffractometer equipped with an Anton Paar HTK1200N furnace at the MIT Center for Materials Science and Engineering. The patterns obtained on this instrument were analyzed using the Rietveld software as part of the X'pert HighScore Plus analysis package.

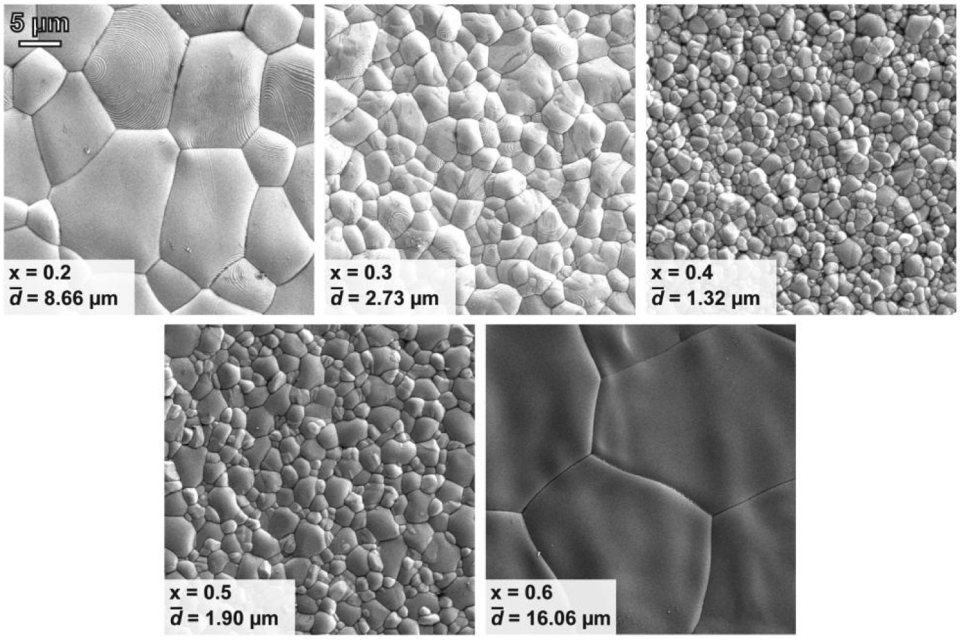

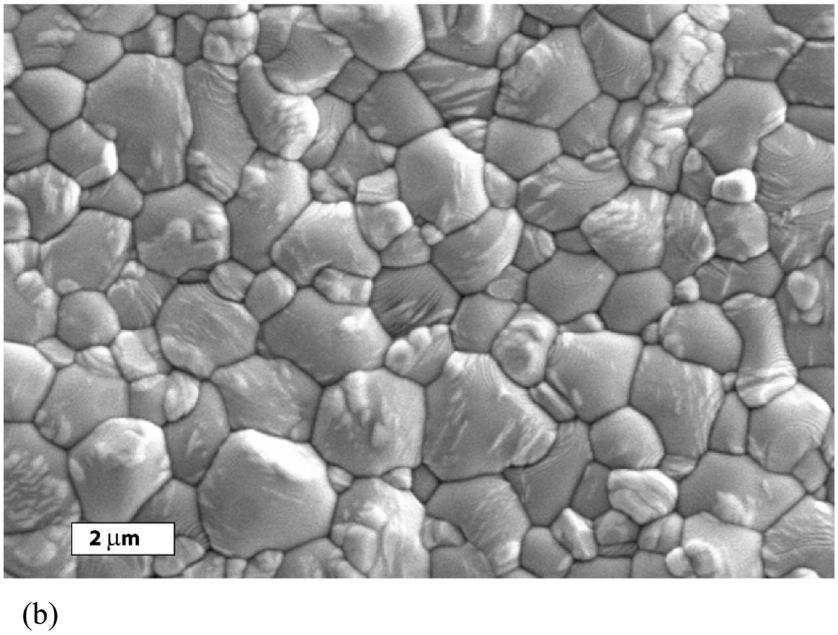

Fig. 2. (a) Comparison of the grain sizes after heating for 40 h at 1600 °C. The grains are largest outside the two-phase region in Fig. 1. Sintered surfaces. All micrographs are the same magnification. (b) Higher magnification of the surface of a x = 0.5 sample after heating for 40 h at 1600 °C. In this back-scatter electron image, bands of a lighter phase are embedded within some of the individual zirconia grains indicating that many individual grains consist of two phases.

High temperature synchrotron studies of the 40, 50 and 60 mol% ZrO_2 compositions were performed at the European Synchrotron Radiation Facility (Grenoble, France) at a wavelength of 0.29419355 Å (42 keV). This high energy was chosen to minimize the absorption by tantalum in the samples. The powders, held in a platinum tube, were heated with a triple lamp furnace to roughly 1700 °C, and diffraction patterns were acquired during subsequent cooling to room temperature. The measurement temperature was determined from the positions of the platinum diffraction lines using the known thermal expansion of platinum [24]. Whole pattern fitting and Rietveld analysis of the acquired synchrotron X-ray data was conducted using the GSAS software [25–27].

To form dense pellets, the calcined powders were ball-milled in ethanol, using 3 mm YSZ balls in an YSZ jar, at 200 rpm for 2 h. The suspension was then allowed to sit for 3.5 h to allow the larger particles to settle out. The smaller particles were isolated by centrifugation and dried overnight. Solid disk pellets were then made by mixing the fine powders with a binder (5 wt% PVA in DI water) and cold, uniaxial pressing the slurry at 700 MPa. Pellets were heated to 700 °C at 2 °C/min and held for 2 h to burn off the binder, then continued ramping at 5 °C/min to 1600 °C and held for 40 h. This procedure was adopted in order to make fully dense pellets since dense pellets could not be made by simply sintering without removing agglomerates. The microstructures were observed by scanning electron microscopy, and EDAX analysis was carried out using a JSM-7200F Schottky FE-SEM.

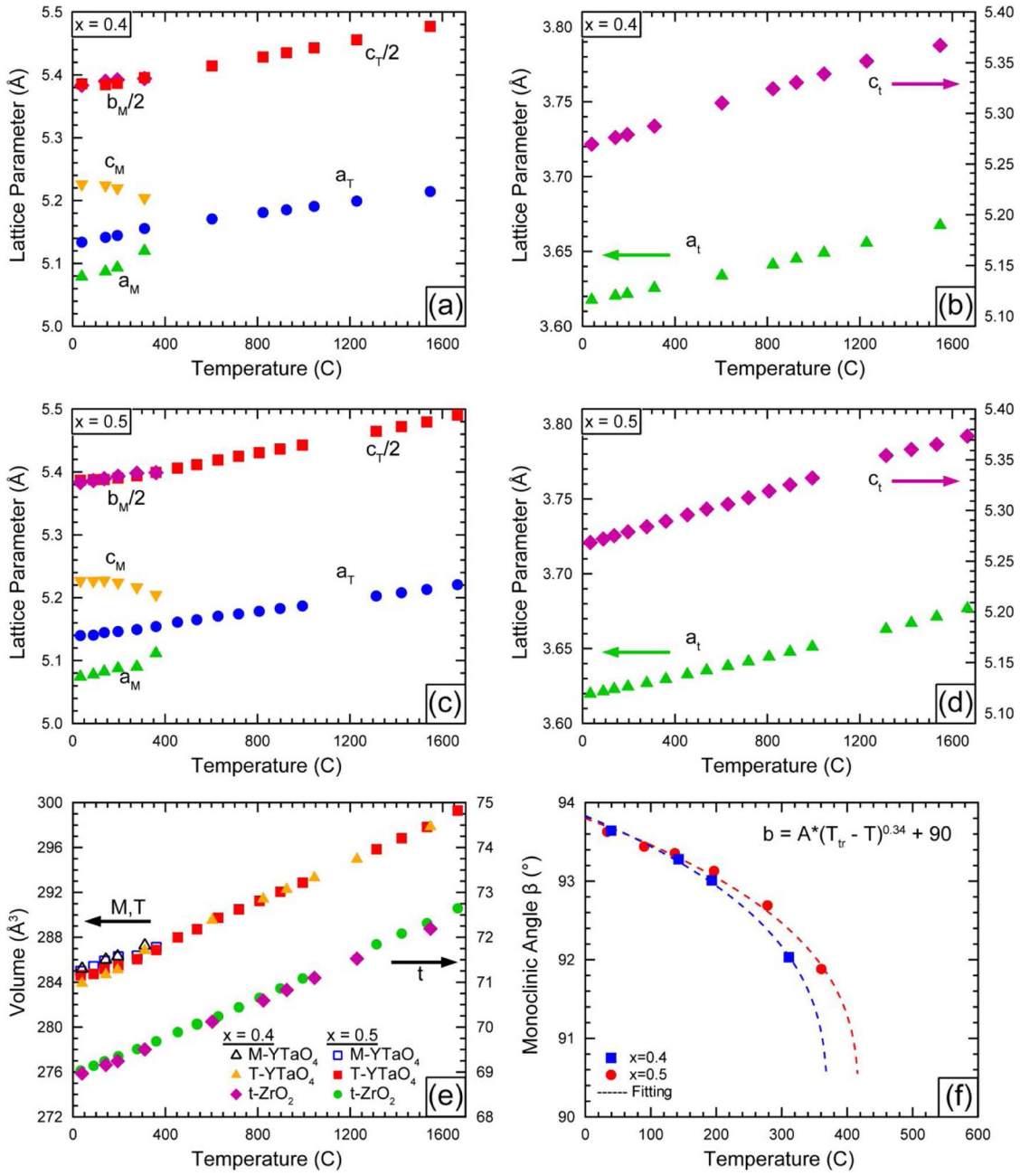

Fig. 3. Unit cell parameters as a function of temperature of the (a) $YTaO_4$ (ss) phase for x = 0.4, (b) ZrO_2 (ss) phase for x = 0.4, (c) $YTaO_4$ (ss) phase for x = 0.5, and (d) ZrO_2 (ss) phase for x = 0.5. Variations in unit cell volumes with temperature for the three phases are shown in (e) for the two compositions. The variation of the monoclinic angle, β, as a function of temperature is shown in (f).

3. Results and observations

Based on the high-temperature X-ray analysis of the powders, two tetragonal solid solution phases, *T* and *t*, are found to be stable at high temperatures. The solubility limits, derived from the variation in lattice parameters with temperature and composition, are shown in Fig. 1. The lattice parameters of the phases in the two-phase field at high temperatures are shown in Fig. 3 for data obtained from compositions x = 0.4 and x = 0.5, approximately mid-way in the two phase field. The lattice parameter data was extracted, using Rietveld analysis, from the synchrotron measurements made as a function of temperature on cooling from 1552 °C and 1666 °C for the two compositions. (For clarity of presentation, the lattice parameter data for the tetragonal zirconia phase and the $YTaO_4$ solid solution are shown in separate panels in the figure.) Also, shown is a comparison of the unit cell volumes of the two tetragonal phases as a function of temperature. Strikingly, the volume of the *T*-YTaO4 solid solution unit cell is almost exactly four times larger than the volume of the *t*-ZrO2 solid solution. Similarly, they both have almost the same coefficient of thermal expansion, α, up to 1600 °C:

$$\alpha_a^T = 12.9 \times 10^{-6}; \quad \alpha_c^T = 9.74 \times 10^{-6}; \quad \alpha_a^t = 9.62 \times 10^{-6}; \quad \alpha_c^t = 12.42 \times 10^{-6}\,{}^oC^{-1}$$

where the superscript denotes the phase and the subscript denotes the crystallographic axis.

Because of the small variation of the lattice parameters with zirconia concentration, there are experimental uncertainties as to the precise compositional boundaries of the two tetragonal phases, particularly the solubility of the *t*-ZrO_2 phase. This is illustrated by the data in Fig. 4(a). [28,29] Nevertheless, it is clear that the solubility of

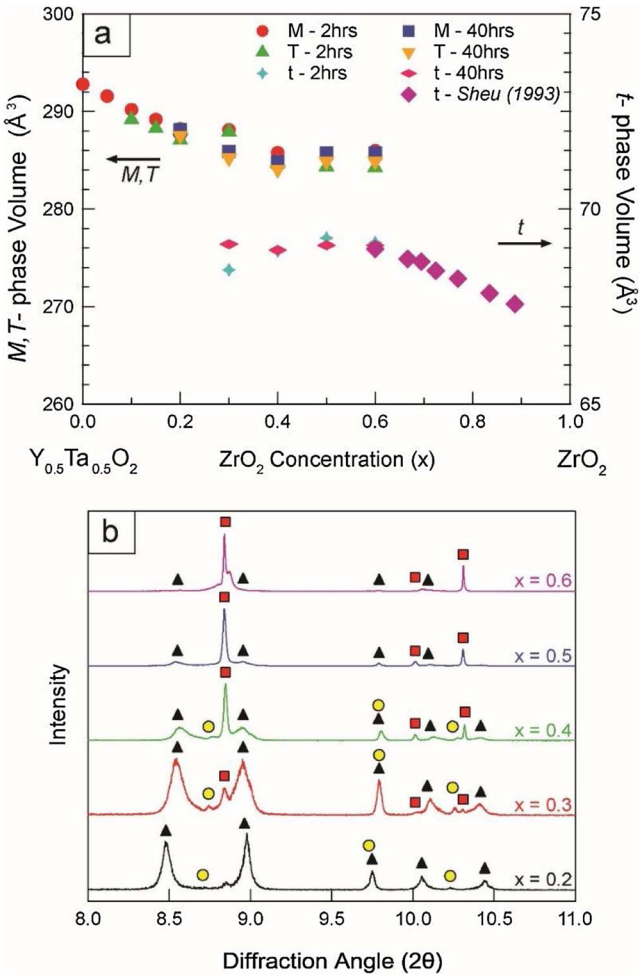

Fig. 4. (a). Variation in unit cell volumes as a function of composition for the*T*, *M* and *t* phases within the two-phase co-existence region. The data for the volumes of the $YTaO_4$ (ss) and ZrO_2 (ss) regions were obtained from literature [1,5]. (b) Room temperature synchrotron scans of the compositions x = 0.2 through x = 0.6, after annealing at 1600 °C for 40 h, showing the phase evolution in the two-phase region. The peaks of the three main phases are indicated by the black triangle (*M*-phase), yellow circle (*T*-phase), and red square (*t*-phase). The *T*-phase is retained from high temperature as a metastable phase (For interpretation of the references to colour in this figure legend, the reader is referred to the web version of this article).

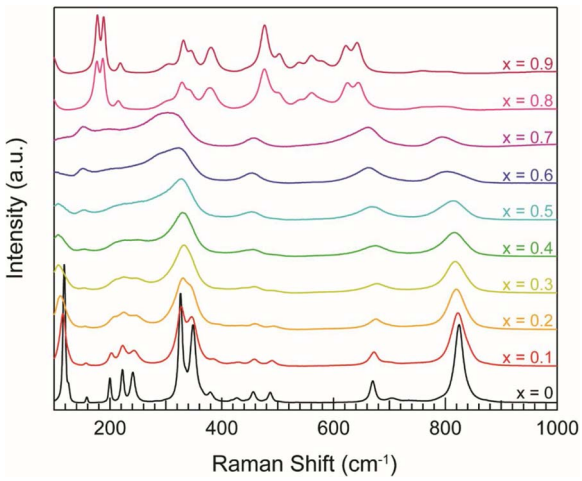

Fig. 5. Raman spectra recorded at room temperature of the indicated compositions across the $YTaO_4$-ZrO_2 system after annealing for 40 h at 1600 °C. The characteristic lines of the monoclinic YTaO4 phase all broaden but do not change with the addition of ZrO_2. The spectra for the two compositions closest to ZrO_2 are characteristic of monoclinic ZrO_2 consistent with the transformation on cooling of the tetragonal ZrO_2 solid solution. In the two-phase region, the lines of both tetragonal solid solution phases have merged and are not distinguishable. Laser excitation 532 nm.

zirconia in $YTaO_4$ is only weakly dependent on temperature from about 450 °C to 1600 °C, the upper limit of the measurement capabilities, whereas the solubility of the *t*-ZrO2 solution varies with temperature. An interesting feature of the data in Fig. 4(a) is the slow evolution of the unit cell volume of the phases in the vicinity of the solubility limit of zirconia in $YTaO_4$ solid solution taking up to 40 h at 1600 °C to equilibrate even in the fine powders used. Raman measurements (Fig. 5) are consistent with the existence of the two solid solution regimes and the intermediate, two-phase region.

In addition to the factor of four between the volumes of the two co-existing tetragonal solid solutions, *T* and *t*, there is also a lattice correspondence between the two tetragonal solid solution phases at high temperatures. This is shown by the X-ray patterns reproduced in Fig. 6. These are discussed later. The same correspondence is evident in the lower temperature diffraction patterns but this one, recorded at 1666 °C, is presented here because it illustrates most clearly that whereas the diffraction peaks from the *t*-phase are sharper and more symmetric, the peaks from the *T* phase are broader and are asymmetric with a tail on the higher diffraction angle side.

The two-phase region at high temperatures persists on cooling to room temperature with the majority of the tetragonal $YTaO_4$ solid solution (*T*) transforming to its monoclinic form and the tetragonal ZrO_2 solid solution (*t*) remaining untransformed. X-ray data for compositions across the two-phase field are shown in Fig. 4(b). Some tetragonal $YTaO_4$ solid solution (*T*) can be retained but the fraction was found to vary from sample to sample, suggesting that the phase was retained metastably. However, no monoclinic ZrO_2 solid solution phase (*m*) was detectable by either X-ray diffraction or Raman spectroscopy within the two-phase solid solution region. The transformation between the tetragonal (*T*) to monoclinic (*M*) phases of the $YTaO_4$ solid solution was found to be reversible and occur over a range of temperature, starting from ~250 °C to completion at approximately 450 °C. The temperature intervals between measurements made using the synchrotron X-ray source were too coarse to identify the transformation temperature with any precision but extrapolating the monoclinic angle determined as a function of temperature, shown in Fig. 3(f), suggests that the transformation temperature is 450 ± 20 °C. The variation of the monoclinic angle β with temperature could be fitted with the power law

$$\beta = A(T_{Tr} - T)^n + 90$$

where A is a scaling factor, T_{Tr} is the transformation temperature, and *n* is the exponent. A value of $n = 0.34$ was used to fit the monoclinic angles for all compositions, and the intercept of the extrapolated fitted curves with the temperature axis gave the transformation temperature. This value of *n* value was chosen based on previous work characterizing the *M*–*T* transition in ZrO_2-doped $YTaO_4$ for lower ZrO_2 content [15]. It is pointed out that the mean field exponent n = 0.5 does fit the data well close to the transition temperature, and using $n = 0.5$ results in transformation temperatures that are about 40–50° higher.

To more closely determine the transformation temperature, measurements of the phase fractions were made at smaller temperature intervals in a laboratory X-ray diffractometer. These are shown in Fig. 7 for a compacted powder sample. In both, the *t*-ZrO_2 concentration, obtained by Rietveld analysis, remains constant with temperature whereas the proportion of the monoclinic and tetragonal phases vary continuously with temperature. The temperature at which the concentrations are equal is arbitrarily denoted as the macroscopic transformation temperature. Three intriguing findings are revealed by these measurements. The first is that there is no hysteresis between heating and cooling. The second is that the transformation temperature is significantly higher (475 °C) in the dense material than that of the powder

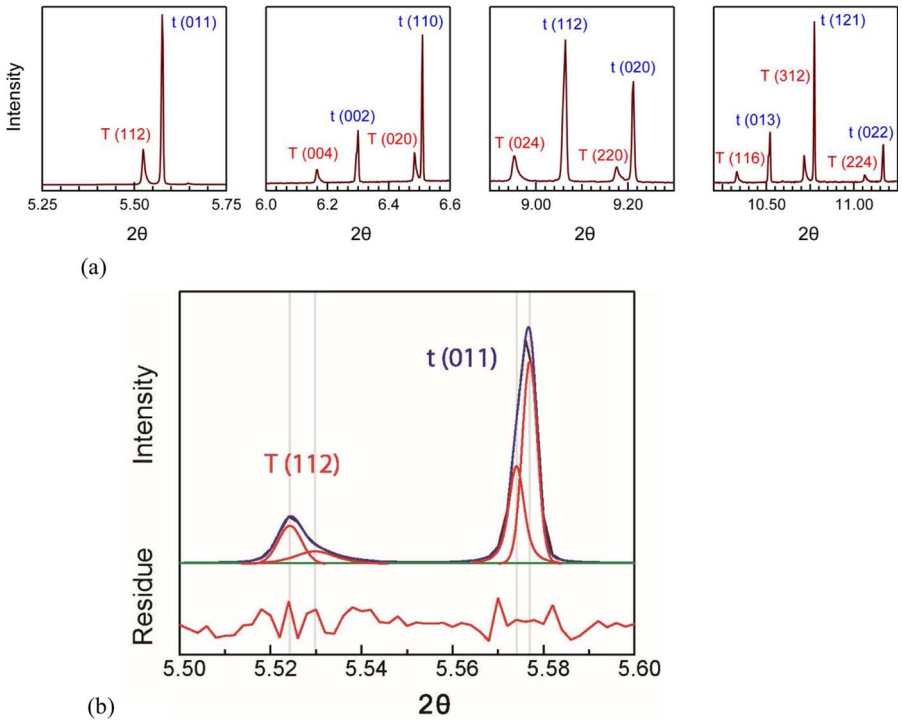

Fig. 6. (a) The principal diffraction peaks of the two tetragonal solid solution phases of the x = 0.5 composition at 1666 °C. Synchrotron data recorded using a wavelength = 0.29419355 Å (42 keV). The Miller indices shown for the two phases are those based on the tetragonal axes of the t-ZrO_2 and *T*-$YTaO_4$ unit cells. (b). Rietveld fits to the T (112) and t (011) peaks. Both peaks display asymmetry due to the presence of a proportion of coherently strained phases. The asymmetry is more pronounced in the diffraction peaks from the*T*-phase but is still discernable for the *t* –phase peaks.

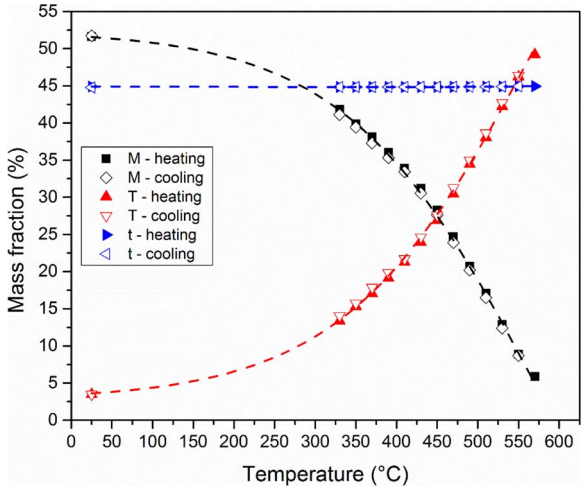

Fig. 7. The fractions of*T* and *M* phases in the two-phase region as a function of temperature on heating and cooling. Powdered sample: 45 m/o ZrO_2. The dashed lines are guides to the eye.

sample (415 °C). The third is the relatively large range of temperatures over which the transformation occurs.

4. Discussion

The phase studies confirm that at temperatures above about 450 °C there is a rather large range of solid solutions extending between the two terminal phases, $YTaO_4$ and ZrO_2, as well as an extended region of two-phase co-existence between these two solid solution phases. The compositional limit of the tetragonal $YTaO_4$ phase is determined from the X-ray diffraction measurements to be ~28 m/o ZrO_2. This is close to that predicted based on first-principles computations (24–25 m/o ZrO_2) [30]. As far as the authors are aware, no computational investigations have been reported of the tetragonal ZrO_2 solubility limit. The value of 65 m/o ZrO_2 is consistent with previous work [15] showing that compositions containing 71.5–73 m/o ZrO_2 are tetragonal but will transform to the monoclinic phase on cooling to liquid nitrogen temperatures.

The two tetragonal solid solution phases are closely related as shown by the small differences in the corresponding peak positions of the *t*- and *T*-phase XRD peaks (Fig. 6). (By way of explanation, the Miller indices for the *t*-ZrO2 solid solution phase peaks are different from those of the T-YTaO4 solid solution phase because the unit cells for the two terminal tetragonal phases are defined in different coordinates). Not only is the *T* unit cell four times the volume of the *t* unit cell but it is also rotated by 45 degrees about their common c-axis. The *T*-phase is equivalent to four unit cells of the t- phase, with two stacked on top of another two in the c-direction, and the *t*-phase being offset from the *T*-phase by a rotation of 45° about the common c-axis (Fig. 8). The lattice correspondence can be expressed as

$$\begin{pmatrix} a_t \\ b_t \\ c_t \end{pmatrix} = \frac{1}{2}\begin{bmatrix} 1 & 1 & 0 \\ -1 & 1 & 0 \\ 0 & 0 & 1 \end{bmatrix}\begin{pmatrix} a_T \\ b_T \\ c_T \end{pmatrix}$$

The origin of the factor of four larger unit cell of the *T* unit cell is attributed to the fact that the symmetry elements of the *T*-phase include a four-fold screw axis. The difference in atomic spacing between the *T*- and *t*- phases is only 0.4% in the c-plane and 2.1% in the *c*-axis direction in the *T*-phase at high temperatures.

As remarked in the results section, a feature of the high temperature tetragonal diffraction peaks is their pronounced asymmetry (Fig. 6). Asymmetry in the *T*- $YTaO_4$ solid solution peaks is more evident but is also observable for the *t*-phase but on the low-angle side of the diffraction peaks. Rietveld decomposition of the peaks, as in Fig. 6(b), shows that the asymmetry is on the high-angle side of the peaks from the *T*-$YTaO_4$ solid solution but on the low angle side of the *t*-phase. The asymmetry would suggest the presence of a secondary *t*-phase containing excess Y^{3+} and Ta^{5+} ions since the volume of the *t*-phase increases with $YTaO_4$ content. The asymmetry in the diffraction peaks from the *T*- and *t*- phases is observed in both the 40 and 50 m/o ZrO_2 samples. In making the argument that the tetragonal $YTaO_4$ phase is stabilized by the simultaneous replacement of one Y^{3+} and one Ta^{5+} by two Zr^{4+} ions it is assumed that the substitutions occur randomly throughout the material. Although such a random substitutional model

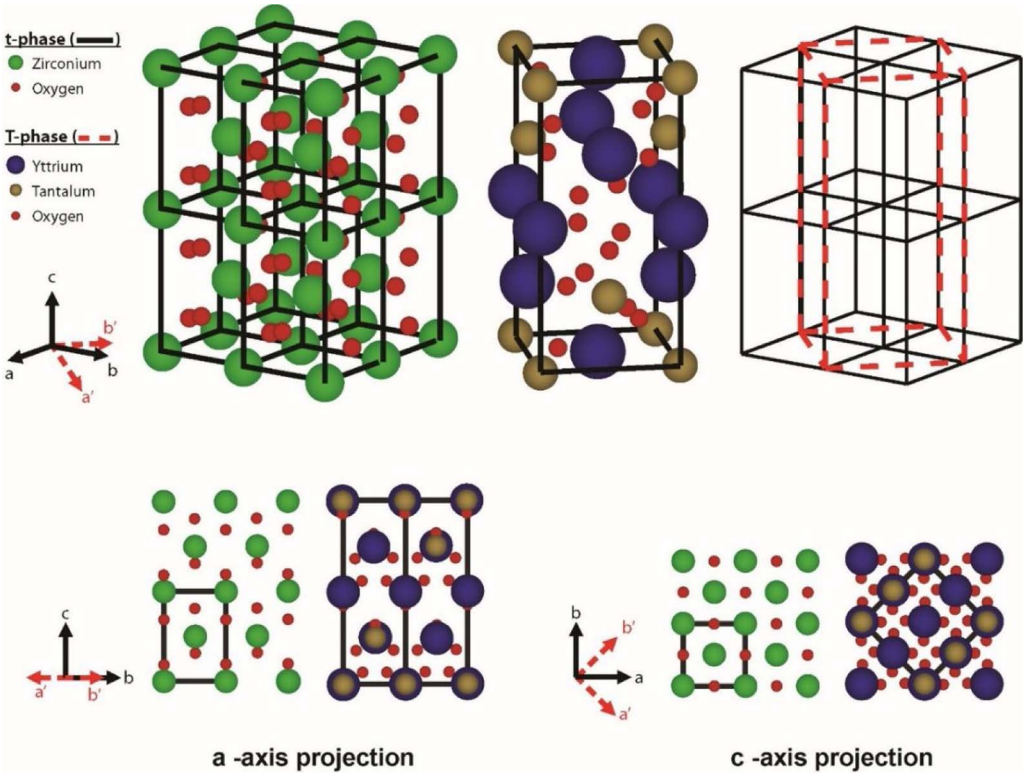

Fig. 8. Comparison of the atomic arrangements in the *T* and *t*- solid solution phases at 1666 °C for the 50 m/o ZrO_2 composition. The *t*-phase structure shown consists of 8 unit cells, while the *T*-phase structure is a single unit cell. The correspondence between the two structures is that the *T*-phase is rotated by 45° about the common c-axis. The superimposition of the *T*-phase unit cell (dashed red) on the eight *t*-phase unit cells (solid black) demonstrates the relationship between the two structures. The volume of one T-phase unit cell is approximately four times the volume of one t-phase unit cell. In the *T*-phase, yttrium and tantalum occupy 36% of the cation sites each, and zirconium occupies 28% of the sites. In the *t*-phase, zirconium occupies 66% of the cation sites, and yttrium and tantalum occupy 17% each. For simplicity in the illustration, zirconium atoms were placed on every cation site in the *t*-phase, while yttrium and tantalum atoms were placed on every site in the *T*-phase. The unit cell lattices are drawn on the basis that the cation sub-lattice of each phase determines the orientation relationships (For interpretation of the references to colour in this figure legend, the reader is referred to the web version of this article).

may be an appropriate assumption at low concentrations, it is likely that it becomes progressively less valid with increasing solute concentration since the substitutional ions are closer together and this presumably influences further substitution. Consequently, some form of preferential clustering of similar (or dissimilar) ions will likely occur by long-range interatomic interactions without altering the net charge neutrality condition and without changing the space group. The observation that the asymmetry is on the high-angle side of the diffraction peaks suggests that the clustering causes some unit cells to contract. As the tetragonal unit cell contracts with increasing ZrO_2 concentration (Fig. 4) this, in turn, suggests that the asymmetry is associated with preferential clustering of the Zr^{4+} ions.

The low temperature tetragonal-monoclinic transformation in the two-phase region of the diagram is unusual because of the absence of any hysteresis on heating and cooling. However, it is consistent with the finding that the transformation in the single phase solid-solution region is characteristic of a second-order displacive ferroelastic transformation with little or no volume change. The finding that the mid-point temperature is higher in solid samples than in powders, is indicative of the transformation being affected by elastic constraints. Although the nature of the constraints is not known, it is likely that it is due to some degree of coherency between the *T* and *t*- solid solution phases. Similarly, the distribution in transformation temperatures, more characteristic of a nucleation and growth transformation, is most likely to be due to distributions in grain sizes and the size of the *T*-$YTaO_4$ solid solution particles embedded within the tetragonal zirconia solid solution grains.

Turning to the bulk materials, the microstructures shown in Fig. 2 are consistent with the existence of a two-phase region. The grain size is smallest and fairly uniform for the 40 m/o ZrO_2 composition close to the center of the two-phase region, but becomes larger and more varied in size as the solubility limits are approached in either direction. In addition, backscattered SEM images show the presence of two different phase regions. The lighter grains correspond to the $YTaO_4$ solid solutions and the darker regions are ZrO_2 solid solution phases; as tantalum has a higher atomic mass it appears lighter in the back-scattering imaging mode of the SEM. This is confirmed by the EDAX mapping images (not shown). One of the curious features of the microstructures in the two-phase field is shown in Fig. 2(b) where some of the darker Zr-rich grains appear to have embedded with them regions of a lighter banded structure. Unlike a typical eutectoid transformation microstructure, in which the eutectoid grows into one of the phases from the grain boundaries, these images suggest that the $YTaO_4$ solid solution phase only grows into the ZrO_2 solid solution phase. There are no corresponding regions where the ZrO_2 solid solution phase is seen to be growing into the grains of the $YTaO_4$ solid solution phase. This conclusion is confirmed by the EDAX mapping which shows unequivocally that the Y and Ta are diffusing into the ZrO2 solid solution phase without any corresponding enrichment of the Zr. Detailed description of the microstructural development leading to these unusual banded microstructures within individual grains is beyond the scope of this contribution but will be published elsewhere.

Finally, based on the shape of the solvus lines of the two-phase region and the close correspondence of the crystallography of the phases, it is possible that there is another, still higher temperature phase transformation above 1700 °C. Given the similarity of the atomic structures of the two tetragonal solid solutions, it is tempting to suggest that they may be related by a phase separation process, such as spinodal decomposition, from a still higher temperature tetragonal phase. It is also possible that the two tetragonal phases form by phase separation from an underlying higher temperature cubic phase; both tetragonal solid solutions phases are different distributions of ions on a cation sublattice with an approximately cubic arrangement of close-packed oxygen ions. Pertinent to this discussion is the phase stability of the $YTaO_4$ at the highest temperatures and continuity of the phases between $YTaO_4$ and ZrO_2 just below their melting temperatures. Above 2350 °C, pure ZrO_2 transforms from tetragonal to cubic before melting at 2715 °C. With stabilization by Y^{3+} alone, the cubic phase extends into a phase field. Whether there exists a corresponding cubic form of the other terminal phase, $YTaO_4$, at the highest temperature is not known but also does not appear to have been studied in detail. If there were a high-temperature cubic phase it would be tempting to surmise

that there would also be a cubic phase above 1700 °C at compositions between the two end member compounds. If pure $YTaO_4$ does not exhibit a cubic phase, then there is unlikely to be a continuous solid solution between it and ZrO_2 at the highest temperatures. Given the close correspondence in crystal structures between the two solid solution tetragonal phases reported here, it is highly likely that there is a phase separation reaction at a higher temperature than can currently be reached.

5. Closing remarks

The phase diagram for the $YTaO_4$-ZrO_2 quasi-binary has been determined up to approximately 1600 °C. There are three distinct compositional regimes: an extensive $YTaO_4$ solid solution, an extensive ZrO_2 solid solution and a two-phase intermediate region. The addition of ZrO_2 to $YTaO_4$ decreases the *M–T* transition temperature almost linearly from 1426 °C to approximately 450 °C at the solubility limit (~28 m/o ZrO_2), and then remains constant until the ZrO_2(ss) phase boundary is reached. Within the intermediate region, there exists an extensive two-phase tetragonal ($T + t$) phase field above the M–T transformation temperature. This is a promising compositional range for TBC applications since the phases are exceptionally stable to grain growth and the absence of compositional vacancies implies very low sintering rates. No other high temperature phases were observed in this region, but it is suggested that there exists a higher temperature solid solution phase is likely above 1700 °C, given the crystallographic relationship between the two tetragonal solid solution structures. Exploring the higher temperature region (above 1600 °C) of the phase diagram and understanding the phase banding which occurs in the intermediate region will be the focus of future work.

Acknowledgements

The authors are grateful to the Office of Naval Research for support of this research under grant N00014-15-1-2715. They are also indebted to DOE-APS for access to the Advanced Photon Source. LL wishes to thank both Region Rhone-Alpes (CMIRA grant 14.004457) and the French Ministry of Defense (DGA-ERE grant 2014.60.0080) for their support while she was at Harvard University.

References

[1] D.R. Clarke, M. Oechsner, N.P. Padture, Thermal-barrier coatings for more efficient gas-turbine engines, MRS Bull. 37 (10) (2012) 891–898.
[2] R.C. Reed, The Superalloys: Fundamentals and Applications, Cambridge University Press, Cambridge, 2006.
[3] J.-C. Han, S. Dutta, S. Ekkad, Gas Turbine Heat Transfer and Cooling Technology, 2nd ed., CRC Press, Taylor & Francis Group, Boca Raton, FL, 2013, p. 869.
[4] Turbine aerodynamics, heat transfer, materials, and mechanics, Progress in Astronautics and Aeronautics Vol. 243 American Institute of Aeronautics and Astronautics, Inc., Reston, VA, 2014, p. 684.
[5] U. Schulz, et al., Some recent trends in research and technology of advanced thermal barrier coatings, Aerosp. Sci. Technol. 7 (2003) 73–80.
[6] J.A. Krogstad, et al., Phase stability of t′-zirconia-based thermal barrier coatings: mechanistic insights, J. Am. Ceram. Soc. 94 (2011) s168–s177.
[7] D.R. Clarke, C.G. Levi, Materials design for the next generation thermal barrier coatings, Annu. Rev. Mater. Res. 33 (1) (2003) 383–417.
[8] A. Limarga, D.R. Clarke, The grain size and temperature dependence of the thermal conductivity of polycrystalline, tetragonal yttria stabilized zirconia, Appl. Phys. Lett. 98 (2011) 211906.
[9] F.M. Pitek, C.G. Levi, Opportunities for TBCs in the ZrO2–YO1.5–TaO2.5 system, Surf. Coat. Technol. 201 (12) (2007) 6044–6050.
[10] V. Lughi, D.R. Clarke, High temperature aging of YSZ coatings and subsequent transformation at low temperature, Surf. Coat. Technol. 200 (5–6) (2005) 1287–1291.
[11] A.M. Limarga, et al., The use of Larson-Miller parameters to monitor the evolution of Raman lines of tetragonal zirconia with high temperature aging, Acta Mater. 59 (2011) 1162–1167.
[12] X.Q. Cao, R. Vassen, D. Stoever, Ceramic materials for thermal barrier coatings, J. Eur. Ceram. Soc. 24 (1) (2004) 1–10.
[13] G.M. Wolten, A.B. Chase, Synthetic fergusonites and a new polymorph of yttrium tantalate, Am. Miner. 52 (1967) 1536–1541.
[14] G.M. Wolten, Diffusionless Phase Transformations in Zirconia and Hafnia, J. Am. Ceram. Soc. 46 (9) (1963) 418–422.
[15] S. Shian, et al., The tetragonal–monoclinic, ferroelastic transformation in yttrium tantalate and effect of zirconia alloying, Acta Mater. 69 (2014) 196–202.
[16] A.M. Limarga, et al., Thermal conductivity of single- and multi-phase compositions in the ZrO2–Y2O3–Ta2O5 system, J. Eur. Ceram. Soc. 34 (12) (2014) 3085–3094.
[17] D.-J. Kim, T.-Y. Tien, Phase stability and physical properties of cubic and tetragonal ZrO2 in the system ZrO2–Y2O3–Ta2O5, J. Am. Ceram. Soc. 74 (12) (1991) 3061–3065.
[18] D.-J. Kim, C.R. Hubbard, X-Ray powder diffraction data for tetragonal zirconia solid solutions in system ZrO2-YTaO4, Powder Diffr. 7 (03) (1992) 174–175.
[19] D.J. Kim, J.W. Jang, H.L. Lee, Effect of tetravalent dopants on raman spectra of tetragonal zirconia, J. Am. Ceram. Soc. 80 (6) (2005) 1453–1461.
[20] Y. Shen, et al., Low thermal conductivity without oxygen vacancies in equimolar YO1.5 + TaO2.5- and YbO1.5 + TaO2.5-stabilized tetragonal zirconia ceramics, Acta Mater. 58 (13) (2010) 4424–4431.
[21] J. Feng, et al., First-principles calculations of the high-temperature phase transformation in yttrium tantalate, Phys. Rev. B 90 (9) (2014) 094102.
[22] M.J. Mayo, Synthesis and applications of nanocrystalline ceramics, Mater. Des. 14 (6) (1993) 323–329.
[23] J.P. Jolivet, M. Henry, J. Livage, Metal Oxide Chemistry and Synthesis: From Solution to Solid State, John Wiley and Sons, 2000.
[24] J.W. Arblaster, Crystallographic properties of platinum, Platinum Met. Rev. 41 (1) (1997) 12–21.
[25] B.H. Toby, EXPGUI, a graphical user interface for GSAS, J. Appl. Crystallogr. 34 (2) (2001) 210–213.
[26] H.M. Rietveld, A profile refinement method for nuclear and magnetic structures, J. Appl. Crystallogr. 2 (2) (1969) 65–71.
[27] B.H. Toby, R.B. Von Dreele, GSAS-II: the genesis of a modern open-source all purpose crystallography software package, J. Appl. Crystallogr. 46 (2013) 544–549.
[28] T.-S. Sheu, T.-Y. Tien, I.W. Chen, Cubic-to-tetragonal (t') transformation in zirconia-containing systems, J. Am. Ceram. Soc. 75 (5) (1992) 1108–1116.
[29] T.-S. Sheu, Anisotropic thermal expansion of tetragonal zirconia polycrystals, J. Am. Ceram. Soc. 76 (7) (1993) 1772–1776.
[30] J. Feng, D.R. Clarke, First Principles Calculations of Zirconia Substitution in $YTaO_4$, (2015).